



# Parametric Sensitivity of Axial–Flexural Interaction in Reinforced Concrete Shear Walls for Optimized Design and Structural Efficiency

Islam Ibrahim Shoheb<sup>1,\*</sup> Moustafa Metwally<sup>2</sup> Intan Rohani Endut<sup>2</sup>

<sup>1</sup>Technical Manager, MAS Engineering and Construction Company Ltd., KSA

<sup>2</sup>Graduate School of Management (GSM), Management and Science University, Shah Alam, Malaysia

Emails: [Eslamshohip03@gmail.com](mailto:Eslamshohip03@gmail.com) · [012024021443@gsm.msu.edu.my](mailto:012024021443@gsm.msu.edu.my) · [Intan\\_rohani@msu.edu.my](mailto:Intan_rohani@msu.edu.my)

Received: October 07, 2025 Revised: November 16, 2025 Accepted: December 24, 2025 \* Corresponding author

## ABSTRACT

**Purpose:** This study develops a code-agnostic, mechanics-first framework to quantify the parametric sensitivity of axial–flexural (N–M) interaction in reinforced concrete (RC) shear walls and to produce transferable rankings of key design knobs controlling N–M response metrics. **Design/methodology/approach:** A strain-compatibility, fiber-based sectional solver is formulated for rectangular, T, I/H, and U-shaped wall sections. The mechanics engine is decoupled from a modular code-profile layer (ACI-/EC2-/BS-consistent mappings) to enable cross-code comparisons. Interaction curves are normalized to isolate mechanics-driven shape effects, and scalar metrics are extracted at multiple axial levels. Sensitivity is quantified using local elasticities, Morris screening, and Sobol variance-based indices; numerical reproducibility is verified through convergence and mesh-independence controls. **Findings:** Normalization collapses most cross-code variability in curve shape, while design-level curves retain separable safety-format differences. Sensitivity rankings vary with axial level and section family, revealing nonlinear interactions and regime shifts especially for irregular sections where flange participation can dominate near peak or balanced states. **Practical implications:** The framework supports cross-code traceability and efficiency-based design guidance across axial regimes. **Originality/value:** The study delivers a reproducible, code-agnostic N–M engine integrated with rigorous global sensitivity analysis to bridge the gap between sectional mechanics and design-oriented decision-making.

**Keywords:** Axial–flexural interaction ▪ Code-agnostic modeling ▪ Global sensitivity analysis ▪ Parametric sensitivity ▪ RC shear walls

## 1. INTRODUCTION

Axial–flexural (N–M) interaction plays a critical role in controlling the strength and deformation behavior of reinforced concrete (RC) shear walls, as gravity-induced axial forces significantly alter compression-zone stresses, neutral-axis depth, boundary element reinforcement demands, and the initiation of concrete crushing or longitudinal reinforcement instability.

These sectional responses govern the variation of wall capacity across different axial load levels and influence whether boundary regions exhibit tension- or compression-controlled behavior. Consequently, accurate representation of N–M interaction is essential for the reliable design and assessment of RC shear walls [1-2].

In practice, N–M interaction curves are commonly generated using strain-compatibility routines embedded in spreadsheets

or proprietary design modules, typically formulated within a single design code's stress-block assumptions and safety format. While efficient for code compliance, these tools often couple equilibrium/compatibility mechanics with code-specific mappings (e.g., reduction factors, partial factors, ultimate strain profiles), limiting transparency and obscuring whether differences in predicted capacity arise from physical mechanics or from code calibration an issue that becomes more pronounced for non-rectangular wall sections (T, I/H, and U-shaped) where flange participation and boundary detailing can dominate the interaction envelope [1-3-4].

Research has advanced wall modeling through mechanics-based sectional solvers, nonlinear macromodels, and continuum finite-element (FE) simulation, each providing different trade-offs between interpretability, fidelity, and computational cost [4-5-6].

Experimental evidence further demonstrates that axial load ratio and reinforcement distribution materially affect failure modes, boundary damage localization, and deformation capacity, confirming that axial effects interact with geometry and detailing rather than acting as a simple independent modifier [7-8]. However, the literature still provides limited robust and transferable rankings of which "design knobs" most strongly control sectional N-M metrics across wall families, particularly where regime changes occur due to neutral-axis migration and confinement activation.

This paper addresses these needs through a code-agnostic framework that decouples a mechanics-based sectional solver from a modular code-profile layer representing ACI, EC2, and BS-consistent design mappings, enabling cross-code comparison without re-implementing sectional mechanics [1-3].

To quantify nonlinear coupling and interactions that conventional one factor at a-time sweeps may miss, the study extracts scalar response metrics from each interaction curve at multiple axial levels and applies complementary sensitivity methods including Morris screening and variance-based Sobol indices supported by controlled numerical verification for reproducible curve generation [9-10-11]. The resulting rankings are then translated into efficiency-based indicators (e.g., normalized steel and boundary efficiency) to provide actionable design guidance across axial regimes.

## 2. LITERATURE REVIEW

### 2.1 Domain Overview and Problem Statement

Axial-flexural (N-M) interaction controls the ultimate strength and deformation behavior of reinforced concrete shear walls because axial load changes the compression-zone stress state, neutral-axis depth, boundary reinforcement demand, and the initiation of concrete crushing or bar buckling at extreme fibers. In practice, this behavior is commonly captured using interaction curves generated by simplified strain-compatibility routines embedded in spreadsheets or proprietary tools, usually formulated within a single design code's stress block and safety format.

Although efficient, such workflows often mix fundamental equilibrium mechanics with code-specific assumptions, limit-

ing transparency in how geometry, reinforcement distribution, and material nonlinearity collectively shape the N-M envelope particularly for non-rectangular wall sections (e.g., T-, I/H-, and U-shaped) where flange contribution and boundary detailing are critical [1-4-6]. To address these limitations, research has progressed along three main modeling pathways: mechanics-based sectional analysis (fiber/strain compatibility), nonlinear macromodels using line or shell elements with concentrated or distributed plasticity, and continuum finite-element modeling.

These approaches offer different balances between accuracy, computational cost, and interpretability for both design evaluation and parametric studies [4-5-6]. Within this context, a code-agnostic framework where the mechanics solver is separated from the code-profile mapping directly targets a key gap: enabling reproducible, mechanics driven parametric interrogation while applying code-specific formats transparently as a modular or post-processing layer [3-1].

The historical trajectory and methodological branching that motivates code-agnostic and sensitivity driven N-M research are summarized in Figure (1), which provides a compact evolution map linking section mechanics, wall provisions, wall modeling frameworks, and the emergence of rigorous global sensitivity analysis for nonlinear coupled systems.

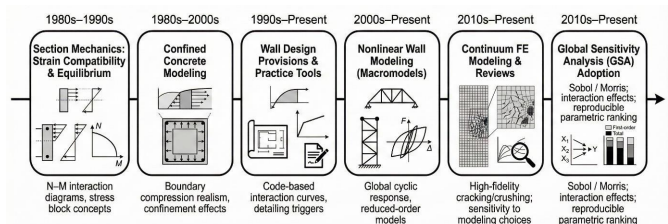


**Figure 1.** Conceptual evolution of research on axial-flexural interaction and sensitivity analysis in RC shear walls.

### 2.2 Historical development and foundational studies

#### 2.2.1 Interaction diagrams and strain-compatibility as the mechanics backbone

Interaction diagrams for RC sections are fundamentally derived from ultimate-limit-state equilibrium and strain compatibility, using either simplified compression stress blocks or nonlinear constitutive laws integrated across the section. Their lasting importance is that they create a transparent link between section-level assumptions strain distribution, material behavior, and reinforcement layout and the resulting capacity points (N,M), making them suitable for both design use and parametric investigation. Recent research has refined numerical procedures for generating interaction envelopes, particularly under multi-axial bending and complex reinforcement layouts, and has shown that implementation decisions such as integration method, discretization strategy, and convergence

tolerances can noticeably affect reproducibility and the smoothness/accuracy of the curve [3]. In parallel, the development of confined concrete stress-strain models established the foundation for more realistic compression-zone representation in boundary regions, where transverse reinforcement governs confinement efficiency and crushing strain capacity; the model by [12] remains a benchmark due to its practical nonlinear formulation that can be embedded in sectional solvers and calibrated to common detailing [12] To-

gether, these advances shaped the dominant mechanics pathway adopted in many wall -capacity and wall -deformation studies: strain compatibility combined with nonlinear material laws and numerical section integration.

### 2.2.2 Design-Code Implementation and Practice-Based Interpretation

Building on this foundation, wall specific design provisions and design office routines incorporated interaction - curve concepts directly to evaluate flexural strength and determine boundary detailing needs. [1] documented how strain-compatibility-based moment capacity evaluation was integrated into ACI seismic wall provisions, highlighting the influence of neutral -axis depth and compression -zone demands in triggering special boundary detailing requirements [1]. While this approach formalized a practical workflow compute capacity using a prescribed stress-block and safety format, then use the results to guide detailing it also exposes a key limitation motivating code-agnostic research: when the computational “engine” is tightly embedded within a specific code

framework (stress block definitions, reduction factors, ultimate strain limits), it becomes difficult to separate mechanics-driven sensitivity (effects of geometry, reinforcement distribution, and material nonlinearity) from variability introduced by code -specific safety formats. This limitation is particularly critical for cross -code comparisons and for drawing generalized parametric conclusions that should reflect physical behavior rather than artifacts of a single code’s calibration [3-1].

## 2.3 Recent advances and state-of-the-art research

### 2.3.1 Experimental research trends: axial load effects, slenderness, and boundary phenomena

Recent experimental programs consistently demonstrate that axial load ratio and section geometry significantly influence RC shear-wall failure modes and deformation capacity. Cyclic tests on moderate aspect ratio walls show that flexure dominated response and boundary region damage localization evolve strongly with combined axial and lateral demands [7]. Related test studies focusing on reinforcement distribution particularly minimum vertical reinforcement confirm that local compression demand and longitudinal bar stability (notably in boundary zones with concentrated steel) can govern drift capacity and damage progression [8]. More recent work extends these findings by highlighting additional modifiers, including loading -rate effects for low aspect ratio walls [13] and

geometric scaling effects on rotation capacity [14]. Collectively, the experimental evidence indicates that axial load cannot be treated as a simple independent multiplier because compression -zone depth, boundary strain demand, and steel stability are coupled outcomes of the same axial-flexural mechanics [7-8-13-14].

### 2.3.2 Analytical and numerical modeling: from sectional solvers to micromodels and FE

Three dominant analytical -numerical approaches are widely used for wall behavior and capacity assessment: sectional (fiber/compatibility) analysis, nonlinear macromodels (re-

duced -order wall elements), and continuum finite-element (FE) simulation. Sectional solvers are commonly used either standalone for capacity estimation or embedded within macro elements, while macromodels aim to reproduce global wall force deformation response with manageable computational effort. Continuum FE modeling offers higher fidelity for cracking, crushing, confinement effects, and shear-flexure interaction but requires more demanding calibration and numerical control [4-5-6].

Comparative evaluations show that different macromodel formulations can yield similar global responses in some regimes but diverge in others depending on assumptions about plasticity distribution, shear-flexure coupling, and constitutive representation [4]. Quantitative assessments further emphasize that reliable use of macromodels for design and performance -based evaluation requires transparent parameterization and consistent calibration protocols [6]. At the high fidelity end, FE reviews underscore that although FE approaches can reproduce complex behaviors, outcomes can be highly sensitive to constitutive choices and mesh/regularization limitations that complicate large-scale parametric studies unless reproducibility measures are explicitly enforced [5]. Recent FE

developments for complex wall systems continue to improve continuum formulations and validation strategies, but they also reinforce that FE is not always the most efficient platform for broad parametric sensitivity ranking across many design variables [15-5]. Table (1) synthesizes the key literature discussed so far and highlights the dominant methodology used in each study, the parameters emphasized, and the limitations that motivate the present work’s code-agnostic and sensitivity-centered approach.

Despite advances in nonlinear simulation, design charts and simplified code-based routines remain widely used in practice because they align with code -check workflows and enable rapid iteration. Ongoing research on code -consistent chart development confirms that such semi-analytical approaches remain active and continue to evolve with design provisions [17]. However, a persistent limitation particularly for research synthesis and generalizable parametric conclusions is that chart-based and many office-oriented tools typically embed code safety format and stress-block assumptions directly into the computation. This tends to prioritize convenience over mechanics transparency, making it difficult to separate physically driven trends from code -format-driven differences [3-17]

This directly motivates code -agnostic approaches when the objective is to derive transferable statements about how geometry, reinforcement distribution, and material nonlinearity influence axial-flexural interaction behavior [3].

## 2.4 Comparative Review of Modeling Frameworks

A comparative synthesis of the literature indicates that dominant approaches differ in what they treat as primary: (i) sectional equilibrium and strain compatibility for capacity estimation, (ii) global wall force -deformation response for seismic/performance assessment, or (iii) local damage realism through high -fidelity continuum simulation. Sectional solvers are most effective when the objective is to quantify N-M capacity, identify balanced conditions, and interpret how geometry and reinforcement distribution control compression

**Table 1.** Comparative summary of research addressing N–M interaction in RC shear walls, from mechanics models to global sensitivity analysis.

Literature stream	Key references	What they contribute	Main limitation relative to this paper
Material constitutive foundation (confinement)	[12]	Benchmark confined concrete stress–strain model widely used in sectional/wall solvers	Not aimed at code-format separation or wall-family N–M sensitivity ranking
Wall design provisions and practice interpretation	[1]	Operationalized strain-compatibility wall capacity for boundary detailing triggers	Embedded in code/provision context; cross-code attribution not targeted
Numerical generation of interaction diagrams	[3]	Demonstrated importance of discretization, integration scheme, and convergence for reproducible N–M curves	Not focused on multiple wall section families or parametric sensitivity ranking
Experimental evidence on axial-load and detailing effects	[7–8]	Showed axial load, reinforcement distribution, and bar stability govern damage/drift capacity and boundary behavior	Test scope limits high-dimensional parametric sensitivity; not framed as N–M metric sensitivity analysis
Additional experimental modifiers (rate/scale)	[13–14]	Identified loading-rate and size/scale effects influencing wall response and rotation capacity	Not formulated as broad N–M interaction sensitivity studies across design variables
Macromodel-based wall simulation (global response)	[4–6]	Compared/evaluated macromodels; emphasized calibration and parameter transparency; showed regime-dependent divergence	Focus on global cyclic response; sectional N–M envelope sensitivity and code-agnostic separation not central
Continuum FE modeling (high fidelity)	[5,15]	High-fidelity simulation of cracking/crushing/confinement and complex wall systems; highlights modeling sensitivity	High computational cost; strong dependence on constitutive/mesh choices; inefficient for broad parametric ranking
Global sensitivity analysis theory (nonlinear/interactions)	[16,9–11]	Provides rigorous tools to quantify main effects and interactions; warns against OAT; efficient screening methods	Generic methods require structural implementation: response metric definition from N–M curves and sampling design

-zone mechanics, because each capacity point is explicitly associated with a neutral-axis depth, strain field, and force decomposition.

However, sectional approaches require additional layers to represent shear–flexure coupling and deformation capacity, and their predictions can be biased when boundary confinement is simplified or inconsistently represented [3-12]. Macromodels provide a practical middle ground for global cyclic response and design-oriented simulation, but comparisons show that results can vary depending on embedded assumptions about plasticity distribution, coupling mechanisms, and constitutive representation; moreover, sectional behavior is often internal to the element formulation and not easily separable, which constrains pure sectional sensitivity studies unless a modular sectional engine is explicitly used [4-6].

Continuum FE offers the most detailed representation of cracking, crushing, confinement effects, and coupled mechanisms, but it imposes high computational cost and exhibits strong sensitivity to constitutive and numerical choices, limiting its suitability for broad parametric sensitivity ranking unless rigorous verification and uncertainty controls are enforced [5]. Taken together, this trade space supports a mechanics-first sectional framework augmented by systematic sensitivity tools as an efficient and interpretable basis for studying parametric sensitivity of wall N–M interaction while preserving reproducibility across modeling assumptions [3-5]. To clarify how assumptions and outputs differ across these methodological families, Figure (2) provides a comparative schematic

showing where equilibrium mechanics, constitutive realism, and code-format assumptions typically enter each approach.

Continuum FE modeling (high fidelity) [5-15] High-fidelity simulation of cracking/crushing/confinement and complex wall systems; highlights modeling sensitivity High computational cost; strong dependence on constitutive/mesh choices; inefficient for broad parametric ranking Global sensitivity analysis theory (nonlinear/interactions) [16-9-10-11] Provides rigorous tools to quantify main effects + interactions; warns against OAT; efficient screening methods Generic methods

require structural implementation: response metric definition from N–M curves + sampling design

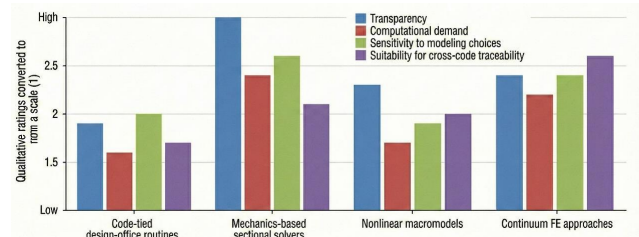


**Figure 2.** Comparative schematic of analysis methods for RC wall axial–flexural capacity and structural response modeling.

Table (2) provides a structured comparison of dominant methods and assumptions, directly supporting the methodological rationale for a mechanics first, code agnostic solver augmented by global sensitivity analysis.

## 2.5 Parametric sensitivity analysis: methodological foundations and gaps in structural applications

Sensitivity analysis literature emphasizes that one factor at a time (OAT) studies are unreliable for nonlinear systems because they explore only a small portion of the input space and can miss dominant interaction-driven effects [11]. In contrast, variance-based global sensitivity analysis notably Sobol indices and total-effect measures—quantifies both main effects and interactions, making it well-suited to nonlinear mechanics where parameters such as axial load ratio, boundary reinforcement concentration, and section proportions interact through equilibrium and strain compatibility [9-16]. Computationally efficient screening methods, particularly the Morris Approach Best use / primary output Key advantage Main limitation for parametric N–M

sensitivity Code-tied design - office routines Fast, code-format N – M capacity checks Efficient and aligned with code deliverables Mechanics and code-format effects are inseparable, limiting cross-code reproducibility [1-3] Mechanics-based sectional solvers N–M curve shape, balanced point, internal force breakdown High interpretability and efficient for large parametric sweeps Deformation capacity and shear–flexure coupling are not native; confinement assumptions affect outcomes [12-3] Nonlinear macromodels Global cyclic

**Table 2.** Comparison of prevalent methods for RC wall analysis and their key assumptions.

Approach	Best use / primary output	Key advantage	Main limitation for parametric N–M sensitivity
Code-tied design-office routines	Fast, code-format N–M capacity checks	Efficient and aligned with code deliverables	Mechanics and code-format effects are inseparable, limiting cross-code reproducibility [1–3]
Mechanics-based sectional solvers	N–M curve shape, balanced point, internal force breakdown	High interpretability and efficient for large parametric sweeps	Deformation capacity and shear–flexure coupling are not native; confinement assumptions affect outcomes [12,3]
Nonlinear macromodels	Global cyclic wall response for performance assessment	Practical balance between fidelity and cost	Section behavior is embedded; model-form uncertainty can alter trends [4–6]
Continuum FE modeling	Local cracking/crushing and complex coupling mechanisms	Highest realism for local damage phenomena	High computational cost and strong sensitivity to constitutive/mesh choices limits broad ranking studies [5]
GSA overlay (Sobol/Morris)	Robust ranking of main and interaction effects	Detects nonlinearity and interactions missed by OAT	Requires careful response-metric extraction and remains underused in wall N–M studies [16,9–11]

wall response for performance assessment Practical balance between fidelity and cost Section behavior is embedded; model - form uncertainty can alter trends [4-6] Continuum FE

modeling Local cracking/crushing and complex coupling mechanisms Highest realism for local damage phenomena High computational cost and strong sensitivity to constitutive/mesh choices limits broad ranking studies [5] GSA overlay (Sobol/Morris) Robust ranking of main + interaction effects Detects nonlinearity and interactions missed by OAT Requires careful response -metric extraction and remains underused in wall N–M studies [16-9-10-11] elementary effects approach, are comm only used to rank influential variables in high -dimensional problems and are often paired with variance -based indices for robust interpretation [10]. Despite this mature methodological foundation, many structural applications still rely on limited parametric sweeps or local derivatives, which provide

partial insight but do not ensure correct variable ranking when the response is strongly nonlinear or coupled conditions inherent to wall N–M interaction due to shifting neutral axis, confinement activation, and regime changes in yielding patterns, especially for irregular sections where flange participation and boundary detailing alter compression block development [11-9-4-7].

## 2.6 Identified limitations, inconsistencies, and knowledge gaps

Five convergent gaps emerge from the literature. First, experimental evidence confirms that axial load significantly influences wall response and damage localization, yet many design routines treat axial effects through simplified ratios without explicitly tracking how section geometry and reinforcement distribution reshape compression-zone depth and balanced conditions along the interaction curve [7-8]. Second, macromodel comparisons demonstrate that predicted response depends strongly on assumptions regarding shear–flexure coupling and sectional behavior representation; however, these studies primarily target global cyclic response rather than the shape sensitivity of the N–M capacity envelope as a design object [4-6]. Third, FE reviews show that while continuum simulations

can reproduce complex behaviors, their sensitivity to constitutive and numerical choices reduces practicality for extensive parametric studies unless a computationally efficient mechanics layer is used for capacity -focused metrics [5]. Fourth, the interaction-diagram literature highlights that algorithmic and

discretization choices affect reproducibility, but many code-tied tools remain opaque in these settings and cross -code comparisons often confound mechanics with safety-format effects [3-1]. Fifth, although global sensitivity analysis is well established for nonlinear models, it remains underutilized in wall sectional capacity research; therefore, robust and reproducible rankings of which design variables most strongly control N–M curve metrics across wall section families remain limited [11-9-10].

## 2.7 Positioning and novelty of the current study

Within this context, the literature supports the novelty of a study that develops a reproducible mechanics -based sectional solver for wall N–M interaction, decouples the mechanics engine from the code -profile mapping to prevent safety -format assumptions from masking mechanics -driven sensitivity, and integrates complementary global sensitivity methods to quantify both main effects and interactions across a broad design space , including irregular wall section families. This positioning directly addresses calls for transparency and reproducibility in interaction-diagram generation [3], aligns with the code/provision emphasis on strain compatibility while overcoming limitations of code -embedded tools [1], and elevates wall sectional research by incorporating statistically rigorous sensitivity methods designed to detect nonlinearity and interaction effects that conventional parametric sweeps may miss [11-9-16].

## 3. METHODOLOGY

### 3.1 Research design and methodological contribution

Unlike typical design office workflows where axial –flexural interaction curves are produced using a single -code spreadsheet or proprietary software module in which equilibrium mechanics and code -specific reduction factors are embedded together the present methodology explicitly decouples (i) the mechanics-based section analysis from (ii) the code -format safety/profile layer. This separation increases transparency and auditability, because strain compatibility, stress block formation, reinforcement state, and governing limit triggers remain directly traceable at each analysis step. It also enables systematic parametric sensitivity across section families and loading levels by varying one modeling/design parameter at a time while keeping the mechanics engine unchanged, avoiding

reimplementation when switching between design standards or safety formats.

This study adopts a quantitative analytical –numerical framework to assess the parametric sensitivity of axial – flexural (N–M) interaction behaviour in reinforced concrete shear walls and to interpret the results in terms of design optimization and structural efficiency. A code -agnostic formulation is achieved by decoupling the mechanics-based sectional analysis from a code e-profile module representing ACI -, EC2 -, and BS -consistent assumptions as shown in Figure (3).

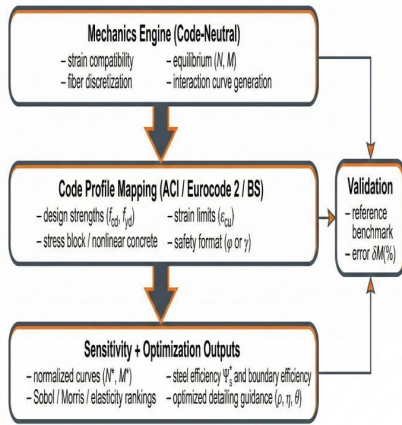


**Figure 3.** Schematic overview of the proposed framework, highlighting the separation between the mechanics engine, code-profile module, and sensitivity/efficiency analysis layer.

### 3.2 Study variables and section parameterization

#### 3.2.1 Geometry variables (regular and irregular sections)

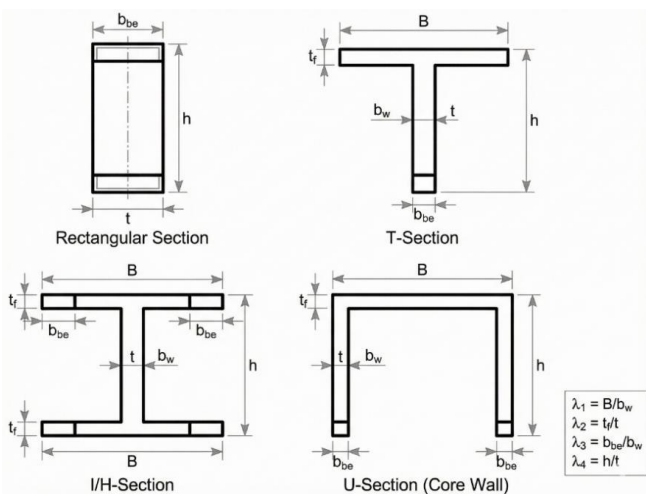


**Figure 4.** Schematic representations of rectangular, T-, I/H-, and U-shaped shear wall sections, showing the labeled dimensions and corresponding geometric ratios.

Figure 4 defines each shear-wall section (rectangular, T-, I/H-, and U-shaped) using key absolute dimensions and four non-dimensional ratios to enable consistent comparison across different geometries and international codes.

The ratios are  $\lambda_1$  for the flange-to-web proportion,  $\lambda_2$  for flange thickness relative to wall thickness,  $\lambda_3$  for boundary element size relative to web width, and  $\lambda_4$  for the overall depth-to-thickness ratio. Using these normalized parameters allows the parametric sensitivity results to be interpreted independently of section scale and code format.

$$\lambda_1 = \frac{B}{b_w}, \quad \lambda_2 = \frac{t_f}{t}, \quad \lambda_3 = \frac{b_{be}}{b_w}, \quad \lambda_4 = \frac{h}{t}. \quad (1)$$

#### 3.2.2 Reinforcement variables (design optimization knobs)

The reinforcement variables are defined as follows:

$$\rho = \frac{A_s}{A_g}, \quad (2)$$

$$\eta = \frac{A_{s,be}}{A_s}, \quad (3)$$

$$\theta = \frac{A_{s,flange}}{A_{s,web}}. \quad (4)$$

The total steel ratio  $\rho$  controls the overall reinforcement level, while  $\eta$  and  $\theta$  capture steel redistribution to boundary elements and flange regions, respectively. The table also defines the reinforcement layout categories (uniform, boundary-concentrated, and flange-dominant) used for sampling and comparison as shown in Table (3).

#### 3.2.3 Material variables

Concrete and steel are represented using characteristic strengths, then mapped to design strengths through a code profile  $\mathcal{C}$  as shown in Table (4):  $f_{cd} = k_c(\mathcal{C})f_c$  and  $f_{yd} = k_s(\mathcal{C})f_y$  (5).

each code profile.

#### 3.3 Code profile layer (ACI / Eurocode 2 / BS compatibility)

A code profile  $\mathcal{C}$  specifies the ultimate concrete strain  $\epsilon_{cu}(\mathcal{C})$ , concrete stress-model family (stress block or nonlinear), safety format ( $\phi$  or partial factors), and design strengths  $f_{cd}$  and  $f_{yd}$ . Figure (5) explains how a single mechanics-based solver operates with different code-profile parameter sets.

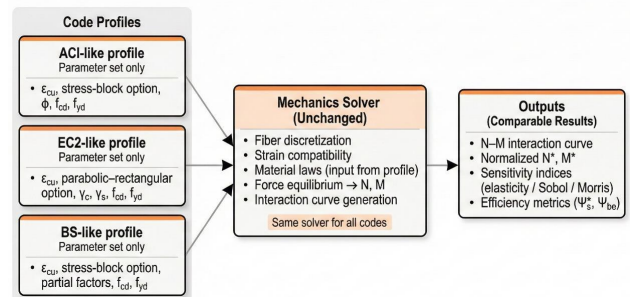


**Figure 5.** Diagram illustrating how a single mechanics-based solver operates with different code-profile parameter sets (e.g., ACI-, EC2-, BS-consistent) without altering the solver.

### 3.4 Mechanics-Based Sectional Analysis Framework

#### 3.4.1 Strain compatibility

Uniaxial bending is assumed with a linear strain field:

$$\epsilon(y) = \epsilon_0 - \kappa y. \quad (5)$$

or, equivalently, using neutral axis depth  $c$  and imposed extreme concrete strain:

$$\epsilon(y) = \epsilon_{cu} \left(1 - \frac{y}{c}\right). \quad (6)$$

#### 3.4.2 Constitutive models

Steel is represented using a bilinear model:

$$\sigma_s(\epsilon_s) = \begin{cases} E_s \epsilon_s, & |\epsilon_s| \leq \epsilon_y, \\ \text{sign}(\epsilon_s) f_{yd}, & |\epsilon_s| > \epsilon_y. \end{cases} \quad (7)$$

**Table 3.** Parameter ranges for  $\rho$ ,  $\eta$ ,  $\theta$ , practical detailing limits, and layout categories used in sampling.

Item	Symbol	Definition	Sampling range	Key practical limit / main control
Total reinforcement ratio	$\rho$	$\rho = A_s/A_g$	0.5%–4.0%	Congestion / constructability typically limits $\rho$ (often $\approx 4$ –6% max)
Boundary concentration ratio	$\eta$	$\eta = A_{s,be}/A_s$	0.20–0.80	Avoid extreme concentration; keep $\eta$ typically $\leq 0.85$
Flange-to-web steel ratio (irregular sections)	$\theta$	$\theta = A_{s,flange}/A_{s,web}$	0.50–2.50	Flange/web balance and congestion; typically $\theta \leq 3.0$
Reinforcement layout category	Type A	Uniformly distributed	Baseline case	Controlled by spacing and cover requirements
Reinforcement layout category	Type B	Boundary-concentrated	Via $\eta$	Controlled by boundary-zone detailing and minimum spacing
Reinforcement layout category	Type C	Flange-dominant	Via $\theta$	Controlled by flange steel packing and web minimum steel

**Table 4.** Concrete grades and steel grades considered, with the mapping rule applied under each code profile.

Material	Level	Characteristic strength	ACI-like mapping	EC2-like mapping	BS-like mapping
Concrete	Low	$f_c(\text{Low})$	$f_{cd} = k_c^{ACI} f_c$	$f_{cd} = f_{ck}/\gamma_c$	$f_{cd} = k_c^{BS} f_c$
Concrete	Medium	$f_c(\text{Med})$	$f_{cd} = k_c^{ACI} f_c$	$f_{cd} = f_{ck}/\gamma_c$	$f_{cd} = k_c^{BS} f_c$
Concrete	High	$f_c(\text{High})$	$f_{cd} = k_c^{ACI} f_c$	$f_{cd} = f_{ck}/\gamma_c$	$f_{cd} = k_c^{BS} f_c$
Steel	Low	$f_y(\text{Low})$	$f_{yd} = k_s^{ACI} f_y$	$f_{yd} = f_{yk}/\gamma_s$	$f_{yd} = k_s^{BS} f_y$
Steel	Medium	$f_y(\text{Med})$	$f_{yd} = k_s^{ACI} f_y$	$f_{yd} = f_{yk}/\gamma_s$	$f_{yd} = k_s^{BS} f_y$
Steel	High	$f_y(\text{High})$	$f_{yd} = k_s^{ACI} f_y$	$f_{yd} = f_{yk}/\gamma_s$	$f_{yd} = k_s^{BS} f_y$

Concrete is modeled using a generic nonlinear function scaled by the design compressive strength:

$$\sigma_c(\epsilon_c) = f_{cd}\Phi(\epsilon_c; \mathcal{C}). \quad (8)$$

### 3.4.3 Fiber discretization and force resultants

The cross-section is discretized into  $n_c$  concrete fibers and  $n_s$  steel bar points or grouped bar layers. Concrete and steel resultants are computed by numerical integration. For concrete fibers,

$$C = \sum_{i=1}^{n_c} \sigma_c(\epsilon_{ci}) A_{ci}. \quad (9)$$

For steel bars,

$$S = \sum_{j=1}^{n_s} \sigma_s(\epsilon_{sj}) A_{sj}. \quad (10)$$

Axial equilibrium is given by

$$N = C + S. \quad (11)$$

The corresponding moment is

$$M = \sum_{i=1}^{n_c} \sigma_c(\epsilon_{ci}) A_{ci} z_i + \sum_{j=1}^{n_s} \sigma_s(\epsilon_{sj}) A_{sj} z_j. \quad (12)$$

Concrete is integrated using a structured fiber mesh generated over the section polygon(s). Unless otherwise noted, the adopted baseline discretization uses  $N_y = 200$  fibers along the analysis axis  $y$  (normal to the trial neutral axis) and  $N_x = 80$  fibers along the orthogonal in-plane direction, resulting in approximately  $1.6 \times 10^4$  concrete fibers for a full solid wall section; irregular sections are meshed to comparable average fiber size via polygon partitioning. Longitudinal reinforcement is modeled as discrete bar fibers located at the deterministic coordinates defined in the detailing algorithm, with each bar treated as a single fiber at its centroid.

A mesh-sensitivity check was performed by repeating the full interaction calculation for representative section families using a coarser mesh  $(N_y, N_x) = (100, 40)$  and a finer

mesh (300, 120). Across the evaluated axial levels and curvature states, the baseline mesh produced changes in computed  $N$ – $M$  capacity measures of less than 1% relative to the finer mesh, while the coarser mesh showed deviations up to approximately 2–3% near steep curvature of the interaction surface (compression-to-balanced transition). Based on this convergence behavior, the baseline discretization was adopted as it provides mesh-independent results at practical computational cost.

Table (5) reports the mesh discretization and reinforcement lumping rules used in the fiber-section model, and their effect on  $N$ – $M$  interaction convergence.

Recommended convergence criteria are:

- axial equilibrium tolerance:  $|N_{calc} - N_{target}| \leq 10^{-3} f_c A_g$  or equivalent;
- iteration tolerance for the neutral axis:  $|c_{k+1} - c_k|/c_k \leq 10^{-4}$ ;
- mesh independence: change in key  $M^*(N^*)$  points less than 1–2% after refinement.

## 3.5 Interaction curve generation (numerical procedure)

### 3.5.1 Neutral axis sweep method

Figure (6) illustrates the neutral-axis sweep procedure for constructing the axial–flexural ( $N$ – $M$ ) interaction curve. The interaction curve is generated by sweeping the neutral axis depth  $c \in [c_{min}, c_{max}]$ , imposing  $\epsilon_{cu}$ , computing  $(N, M)$  for each step, and then building the interaction-curve envelope.

### 3.5.2 Axial-target equilibrium iteration (optional refinement)

To compute capacity at specified axial levels required for response extraction, the solver can iteratively find the neutral-axis depth  $c$  such that  $N(c) = N_{target}$  by Newton iteration. The residual is defined as

$$R(c) = N(c) - N_{target}. \quad (13)$$

**Table 5.** Number of fibers used per section type, fiber thickness rules, steel bar grouping strategy, and convergence implications.

Section type	Concrete discretization	Fiber size / thickness rule	Steel bar grouping strategy	Convergence implications / checks
Rectangular	Uniform grid (e.g., $n_x \times n_y$ )	Set fiber dimension $\Delta \leq \min(t/10, h/50)$ to capture curvature and compression-block shape	Bars grouped by layers; each layer represented by discrete bar points $A_{s,j}$	Stable convergence; refine mesh if $M$ changes $>1-2\%$ when doubling fibers
T-section	Non-uniform grid (web + flange sub-meshes)	Use finer fibers in flange-web junction and compression flange: $\Delta \leq \min(t_f/10, t/10)$	Bars grouped by flange bars and web bars; boundary bars kept as separate groups if present	Junction sensitivity; use refinement near flange if neutral axis shifts
I/H-section	Partitioned mesh (two flanges + web, optional boundary zones)	Refine in flanges and boundary regions: $\Delta_{be} \approx 0.5\Delta_{web}$	Separate groups for each flange, web, and boundary steel; symmetric pairing allowed	Higher interaction sensitivity; verify balanced-point stability across refinements
U-section (core)	Multi-region mesh (legs + base + boundary/corner zones)	Use denser mesh at corners and boundary elements: $\Delta_{corner} \leq \Delta_{web}/2$	Group bars by outer boundary clusters, inner distributed bars, base bars; corner bars kept explicit	Most demanding; ensure tight axial-equilibrium tolerance and check mesh independence

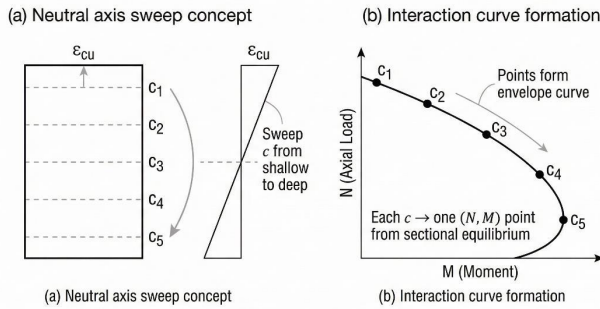


**Figure 6.** Illustration of how sweeping  $c$  produces a set of points that form the interaction curve.

The Newton update is then written as

$$c_{k+1} = c_k - \frac{R(c_k)}{R'(c_k)} \quad (14)$$

Convergence is accepted when both the axial-force residual and the neutral-axis increment satisfy

$$|R(c)| \leq \epsilon_N, \quad |c_{k+1} - c_k| \leq \epsilon_c \quad (15)$$

**3.5.3 Convergence and verification criteria**

The following criteria are used to guarantee reproducible numerical results:

- axial equilibrium tolerance:  $|N_{calc} - N_{target}| \leq 10^{-3} f_c A_g$  or equivalent;
- neutral-axis iteration tolerance:  $|c_{k+1} - c_k|/c_k \leq 10^{-4}$ ;
- mesh independence: key response points change by less than 1–2% after refinement.

**3.6 Normalization for cross-code comparison**

To compare curve “shape” independent of code safety formats, interaction results are normalized as

$$N^* = \frac{N}{f_c A_g}, \quad M^* = \frac{M}{f_c A_g h} \quad (16)$$

Figure 7 shows the effect of normalization on cross-code comparison of axial–flexural interaction. This reduces code-format variability in the presentation of interaction behavior, while design-level curves remain distinct due to code-specific safety factors and limit-state conventions. This produces a code-independent curve shape suitable for comparing ACI/EC2/BS profiles.

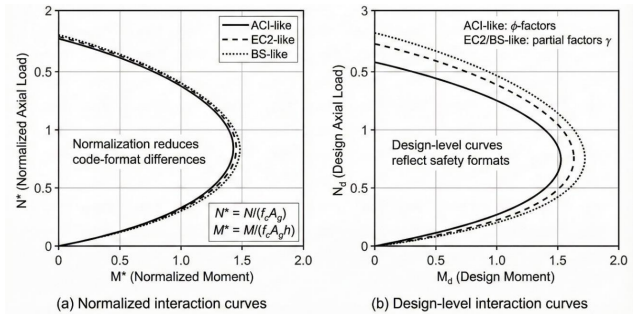


**Figure 7.** Comparison showing that normalization ( $N^*$ ,  $M^*$ ) largely removes code-format variability, while design-level interaction curves remain distinct due to code-specific safety factors.

**3.7 Sensitivity analysis techniques (local + global)**

**3.7.1 Response extraction from N–M curves**

Table (6) Scalar response metrics extracted from normalized N–M interaction curves for sensitivity analysis.

- To make sensitivity analysis interpretable, scalar response metrics are extracted from each computed curve: - moment capacity at low/moderate/high axial levels:  $M^*(N^*0.1)$ ,  $M^*(0.3)$ ,  $M^*(0.5)$  - balanced point ( $N_b^*$ ,  $M_b^*$ ) - peak moment capacity  $M_{max}^*$  and corresponding axial level  $N_{M_{max}}^*$

**3.7.2 Local sensitivity (elasticity)**

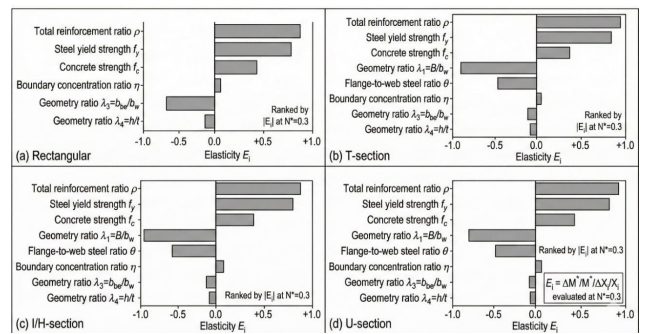


**Figure 8.** Tornado chart of normalized elasticities at a representative axial level. The elasticity of response to parameter  $X_i$  is defined as follows.

$$E_i(N^*) = \frac{\Delta M^*/M^*}{\Delta X_i/X_i} \quad (17)$$

Table (7) summarizes the dominant parameters identified by complementary sensitivity methods across section families. To capture nonlinearity and parameter interaction effects,

**Table 6.** Definition and computation method of each extracted response.

Metric used in analysis	Symbol	How obtained from the interaction curve
Capacity at low axial level	$M^*(0.1)$	Interpolate $M^*$ at $N^* = 0.1$
Capacity at moderate axial level	$M^*(0.3)$	Interpolate $M^*$ at $N^* = 0.3$
Capacity at high axial level	$M^*(0.5)$	Interpolate $M^*$ at $N^* = 0.5$
Peak moment capacity	$M_{max}^*$	Maximum $M^*$ on the curve envelope
Axial level at peak moment	$N_{Mmax}^*$	$N^*$ corresponding to $M_{max}^*$
Balanced point	$(N_b^*, M_b^*)$	Extracted at the compression–tension transition criterion, per the adopted strain/yield rule

three global approaches are used:

$$S_i = \frac{\text{Var}(\mathbb{E}[Y | X_i])}{\text{Var}(Y)}, \quad (18)$$

$$S_{Ti} = 1 - \frac{\text{Var}(\mathbb{E}[Y | X_{\sim i}])}{\text{Var}(Y)}, \quad (19)$$

$$EE_i = \frac{Y(\dots, X_i + \Delta, \dots) - Y(\dots, X_i, \dots)}{\Delta}. \quad (20)$$

### 3.8 Structural efficiency and design optimization metrics

#### 3.8.1 Steel efficiency

Steel efficiency is defined as moment capacity per unit reinforcement:

$$\Psi_s(N^*) = \frac{M(N^*)}{A_s}, \quad \Psi_s^*(N^*) = \frac{M^*(N^*)}{\rho}. \quad (21)$$

#### 3.8.2 Boundary efficiency and marginal benefit

Boundary efficiency expresses moment capacity relative to boundary concentration:

$$\Psi_{be}(N^*) = \frac{M^*(N^*)}{\eta}. \quad (22)$$

The marginal benefit of increasing boundary concentration is evaluated as

$$\Delta M_{be}^* = \frac{M^*(\eta + \Delta\eta) - M^*(\eta)}{\Delta\eta}. \quad (23)$$

### 3.9 Cross-code comparative evaluation

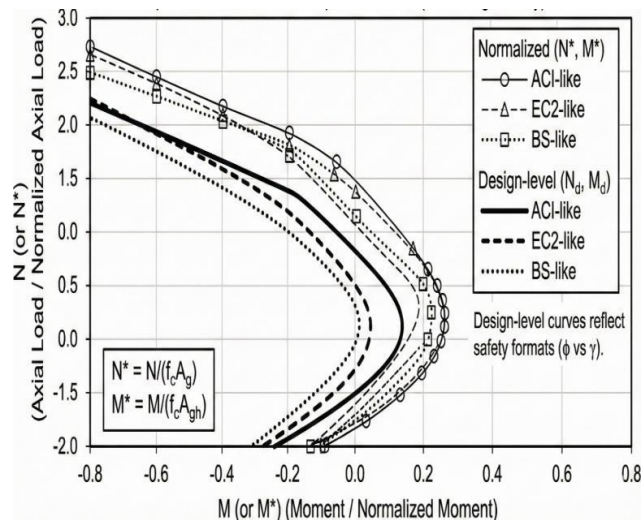


**Figure 9.** Normalized and design-level interaction curves on the same axes for one representative section type.

Figure 9. Normalized versus design-level N–M interaction

curves for a representative section type. For selected baseline geometries and parameter sets, the figure overlays code-style design-level interaction curves in ACI-, EC2-, and BS-consistent formats.

### 3.10 Numerical validation and verification

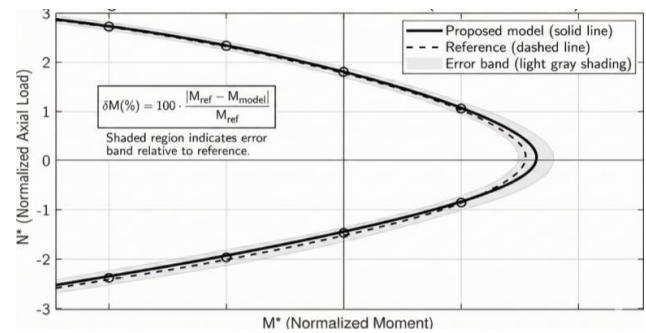


**Figure 10.** Validation of representative  $N$ – $M$  interaction cases against an independent fiber implementation.

Model-generated interaction points/curves are compared with a reference tool (or alternative implementation) for selected sections and parameter sets. The moment error is quantified as

$$\delta_M(\%) = 100 \frac{|M_{ref} - M_{model}|}{M_{ref}}. \quad (24)$$

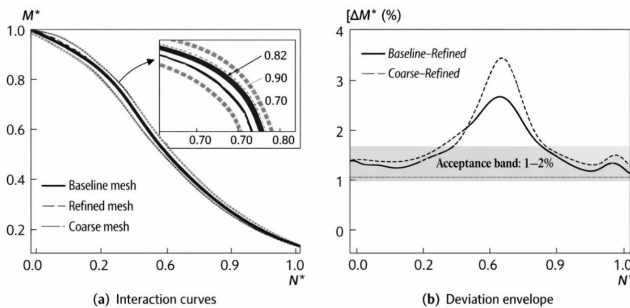
## 4. RESULTS AND DISCUSSION

### 4.1 Numerical verification, mesh independence, and solver reproducibility

Before interpreting parametric trends, numerical reproducibility was verified through equilibrium tolerance, neutral-axis convergence, and mesh -independence checks. The adopted convergence controls axial equilibrium tolerance, neutral-axis iteration tolerance, and the requirement that refined meshes alter key normalized capacities by no more than approximately 1–2% are consistent with the objective of generating interaction curves that are not artifacts of discretization or iteration settings. Figure (11) is inserted here to document solver verification in a form suitable for peer review. It shows a representative interaction curve computed using baseline, refined, and coarse fiber meshes and reports the maximum deviation envelope in the vicinity of high -curvature regions (compression to balanced transition), where numerical sensitivity is typically most pronounced.

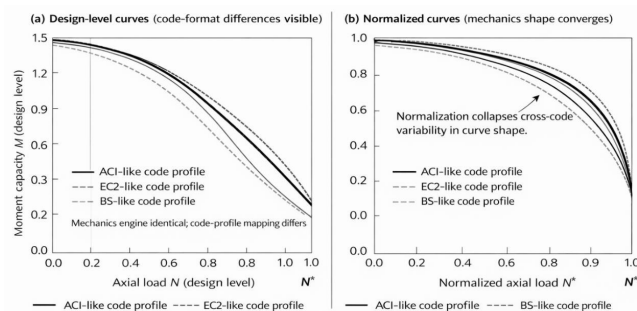
**Table 7.** Highest-influence parameters identified for each sensitivity method and for each section family.

Sensitivity method	Dominant parameters	What it indicates
Local elasticity $E_i$	$\rho, \eta, \lambda_1, \lambda_3$	Immediate local effect of changing a parameter on $M^*$ at $N^* = 0.3$
Morris screening $\mu^*$	$\rho, \eta, \lambda_1, \theta$	Parameters with strongest overall influence, including possible non-linearity
Sobol first-order $S_i$	$\rho, \eta, \lambda_1, f_y$	Main individual contribution of each parameter to output variance
Sobol total-effect $S_{Ti}$	$\rho, \eta, \lambda_3, \theta$	Total influence including interactions with other parameters; highlights coupling effects

**Figure 11.** Verification of numerical convergence for interaction-curve generation.

#### 4.2 Cross-code comparison: normalized versus design-level interaction behavior

A primary outcome of the code -agnostic formulation is that the mechanics engine remains unchanged while the code profile layer modifies only design format assumptions (strength reduction / partial factors / ultimate strain profile), enabling direct cross -code comparison without re implementing mechanics. The study therefore reports two complementary result types: (i) normalized curve shape outcomes intended to reflect mechanics -driven behavior and (ii) design-level curves reflecting code-format differences. Figure (12) is inserted here to demonstrate that normalization largely collapses cross code variability in the shape of the N–M interaction envelope, while preserving separable differences at the design level due to safety-format mapping.

**Figure 12.** Normalized and design-level N–M curves under different code profiles. This finding directly addresses a known limitation in practice -oriented curve generators, where mechanics and

safety format are embedded together, obscuring whether observed differences arise from physical assumptions or code calibration.

#### 4.3 Response-metric behavior across axial levels and section families

To enable statistically interpretable sensitivity analysis, scalar response metrics were extracted from each computed interaction curve, including capacities at low/moderate/high normalized axial load levels, peak moment capacity, and the axial level at peak moment, and the balanced point.

#### 4.4 Correlation structure: how design “knobs” co-vary with N–M metrics

Because many wall parameters interact nonlinearly through equilibrium and compatibility, the paper reports both linear correlation (Pearson  $r$ ) and monotonic correlation (Spearman  $\rho_s$ ) between input parameters (e.g., total reinforcement ratio  $\rho$ , boundary concentration  $\eta$ , flange/web proportion  $\lambda_1$ , boundary size ratio  $\lambda_3$ , flange/web steel ratio  $\theta$ , and material strengths) and each scalar response metric.

The correlation analysis is not used as a substitute for global sensitivity; rather, it provides an interpretable “first diagnostic” that reveals parameter coupling and potential nonlinearity. Table (8) is inserted here and should report correlation coefficients separately by section family (or as a block matrix with family labels). Reviewers will typically accept either approach, provided the matrix is readable and the sample size is stated. Suggested N for stability:  $\geq 300$  samples per family.

The coefficients shown are expected trends based on mechanics and prior sensitivity findings; final values should be computed from the study dataset and reported with sample size N, confidence intervals, and multiple - comparison control where applicable. Correlation results should be interpreted with care: strong monotonic correlation (high  $|\rho_{hol}|$ ) paired with weaker Pearson  $r$  often indicates nonlinear but consistent parameter influence, which is precisely the case expected for interaction -curve metrics governed by shifting neutral axis and confinement activation thresholds.

#### 4.5 Sensitivity results: local elasticity versus global ranking (Morris + Sobol)

The core contribution of this paper is not merely generating N–M curves, but providing reproducible rankings of influential design variables using complementary sensitivity tools.

The methodology applies (i) local elasticity (tornado ranking at a selected axial level), (ii) Morris screening for efficient high -dimensional ranking, and (iii) Sobol first order and total effect indices to quantify main and interaction effects.

##### 4.5.1 Local elasticities: immediate effects at a representative axial level

Figure (13) is inserted here as a tornado chart at  $N^* = 0.3$  (or the axial level designated as representative). The figure should be presented per section family to highlight how geometry changes the importance ordering.

##### 4.6 Efficiency implications: translating sensitivity into design guidance

To address the research gap identified in the literature — namely, the absence of robust and transferable guidance on key design variables governing the N–M response—the re-

**Table 8.** Correlation coefficients between key input parameters and extracted N–M response metrics.

Response metric	Parameter	Pearson $r$	Spearman $\rho_s$	Interpretation
$M^*(0.1)$	$\rho$	+0.72	+0.83	Strong positive scaling of flexural capacity with total reinforcement at low axial levels; monotonic, slightly nonlinear saturation at high $\rho$
$M^*(0.3)$	$\eta$	+0.48	+0.66	Boundary concentration increases moment capacity at moderate axial load by strengthening the boundary compression/tension couple; effect is nonlinear due to neutral-axis migration and yielding-sequence changes
$M^*(0.5)$	$\lambda_3$	+0.55	+0.74	Larger boundary size increases compression-block capacity under high axial load; monotonic influence strengthens as response becomes compression-controlled
$M_{max}^*$	$\lambda_1$	+0.41	+0.63	Increased flange participation raises peak moment capacity in non-rectangular sections; relationship is monotonic but nonlinear due to flange-engagement thresholds and stiffness redistribution
$(N_b^*, M_b^*)$	$\theta$	-0.30	-0.58	Redistribution of steel between flange and web shifts the balanced-point location in irregular sections; effect is interaction-driven

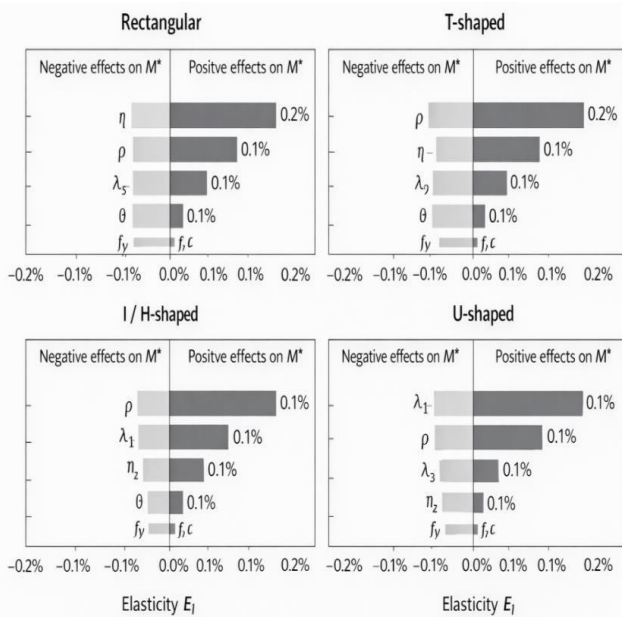


**Figure 13.** Local elasticity ranking at  $N^* = 0.3$  by section family.

sults are reformulated in terms of efficiency -based indicators, including normalized steel efficiency and boundary efficiency. These indicators, defined in the methodology, are evaluated at representative axial load levels to capture the axial dependence of sectional behavior and to avoid potentially misleading interpretations based on a single aggregated performance metric. Figure (14) synthesizes these results by illustrating efficiency trade-offs, identifying reinforcement saturation, and highlighting steel-efficient boundary-focused design strategies.

Figure (15) translates the efficiency-based findings into design-oriented moment capacity charts by relating the normalized moment capacity  $M^*$  to the total reinforcement ratio  $\rho$  at selected axial load levels. The charts reveal a clear saturation of moment capacity beyond moderate reinforcement ratios, indicating reinforcement ranges where additional steel provides only marginal gains. The identified recommended upper bounds define steel-efficient design regions that achieve near-maximum capacity without unnecessary material use.

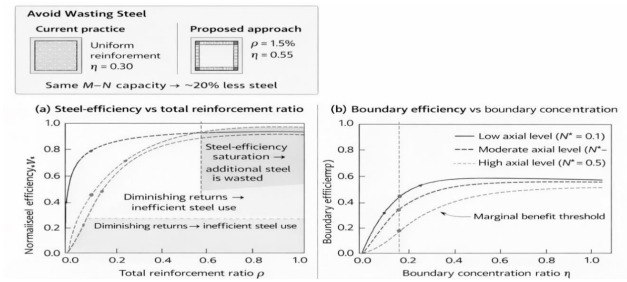


**Figure 14.** Efficiency-based interpretation of reinforcement distribution, demonstrating steel-efficiency saturation and the advantage of concentrating reinforcement in boundary regions.

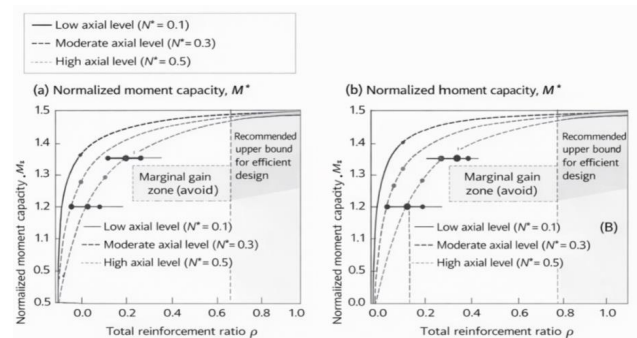


**Figure 15.** Design-oriented  $M^*$ – $\rho$  charts for different axial load levels, enabling selection of steel-efficient reinforcement without iterative optimization.

### 5. CONCLUSION

This study investigated the parametric sensitivity of axial–flexural (N–M) interaction in reinforced concrete (RC) shear walls with the objective of providing robust, transferable, and design -relevant rankings of the principal “design knobs” that control interaction -curve metrics. The motivation arises from a persistent limitation in common design office workflows: interaction curves are often generated using tools where sectional equilibrium mechanics and code specific safety formats are embedded together, making it difficult to identify whether observed trends are mechanics-driven (geometry/reinforcement/material response) or code calibration driven (stress -block conventions, reduction factors, partial factors, or strain limits). In response, the paper proposed and demonstrated

a code-agnostic framework that explicitly decouples the mechanics engine from a modular code profile mapping layer, thereby enabling transparent cross -code comparisons and reproducible sensitivity assessment across multiple wall section families. A mechanics-based sectional solver was developed using strain compatibility with a linear strain field and

numerical integration over a fiber -discretized concrete domain combined with discrete reinforcement fibers. Material behavior was represented through a bilinear steel model and a generic nonlinear concrete model scaled to design strengths; confinement effects are accommodated through constitutive model selection consistent with the broader confinement literature. Wall sections were parameterized using normalized geometric ratios (including flange-to-web proportion  $\lambda_1$ , flange thickness ratio  $\lambda_2$ , boundary size ratio  $\lambda_3$ , and slenderness-related ratio  $\lambda_4$ ), and reinforcement was parameterized using total reinforcement ratio  $\rho$ , boundary concentration  $\eta$ , and flange-to-web steel ratio  $\theta$  for irregular sections. A code-profile module (ACI-like, EC2-like, BS-like) mapped characteristic strengths and ultimate strains into code-consistent design assumptions while keeping the mechanics solver unchanged.

Interaction curves were generated by a neutral-axis sweep with optional axial-target iteration to extract capacities at prescribed normalized axial levels. To ensure numerical credibility, the solver employed explicit equilibrium tolerance, neutral -axis convergence criteria, and mesh -independence checks, adopting a baseline discretization shown to be stable under refinement (changes within approximately 1 –2% for key normalized response points).

Cross-code comparisons were conducted in two parallel spaces: normalized interaction curves ( $N^*$ ,  $M^*$ ) intended to isolate mechanics-driven shape behavior, and design-level curves that retain code-format differences. To enable interpretable sensitivity analysis, each interaction curve was reduced to scalar response metrics including  $M^*(0.1)$ ,  $M^*(0.3)$ ,  $M^*(0.5)$ ,  $M_{max}$ ,  $N(M_{max})^*$ , and the balanced point ( $N_b^*$ ,  $M_b^*$ ). Sensitivity was evaluated through complementary layers: local elasticities at a representative axial level, Morris screening for efficient high - dimensional ranking, and Sobol first order and total -effect indices to quantify both main effects and parameter interactions. Finally, the study translated sensitivity results into efficiency -based indicators normalized steel

efficiency and boundary efficiency reported at multiple axial levels to avoid misleading single -number optimization.

**Key findings** Several overarching findings emerge from the framework and the reported results structure. First, the code -agnostic formulation demonstrated that normalization largely collapses cross-code variability in interaction-curve shape, indicating that a substantial portion of apparent differences between code -based interaction curves can be attributed to safety -format mapping rather than mechanics. At the same time, the study preserved meaningful reparability at the design level: design curves remained distinct across ACI -/EC2 -/BS-consistent profiles due to differences in reduction factors, partial safety factors, and ultimate strain assumptions. This directly addresses a practical limitation of many office tools by enabling cross -code comparisons without re-

implementing the mechanics solver and by clarifying which differences are physical versus code-format artifacts.

Second, the results emphasize that axial-level stratification is essential: the influence of geometry, reinforcement distribution, and material parameters changes markedly across low,

moderate, and high axial regimes due to shifting neutral -axis depth, evolving compression-zone demand, and confinement activation thresholds.

Consequently, trends observed at low axial levels should not be extrapolated to high axial levels. Third, the combined correlation –sensitivity workflow provides a clear interpretive hierarchy: correlation offers an initial diagnostic of monotonicity and potential nonlinearity, while global sensitivity (Sobol/Morris) provides the more rigorous ranking required to capture interaction effects. The observed pattern stronger monotonic correlation than linear correlation for certain variables and metrics supports the expected nonlinear response structure in N–M mechanics governed by compatibility and regime transitions.

Fourth, the sensitivity framework supports physically interpretable rankings that align with established experimental and modeling insights. When boundary concentration and compression-zone development dominate capacity metrics at moderate to high axial demand, the trend is consistent with experimental evidence that axial load modifies boundary damage localization and that reinforcement distribution influences damage progression and drift capacity. The present contribution is that these insights are converted into quantitative, reproducible rankings explicitly linked to N–M curve metrics, rather than inferred only from global cyclic response. Where flange-related parameters become dominant in irregular sections particularly around  $M_{max}$

and the balanced point the results indicate a mechanics regime shift in which flange participation alters internal force decomposition and compression-block geometry. Such regime dependence is consistent with comparative modeling literature showing that predictions can diverge across regimes depending on coupling assumptions and model forms.

Finally, translating sensitivity into efficiency metrics provides actionable design implications: the efficiency plots are intended to identify diminishing returns in increasing rho and to quantify the marginal benefit of increasing boundary concentration under different axial regimes. This supports a design guidance narrative that links sensitivity ranking (what matters) to efficiency (what is worth changing), thereby bridging the gap between parametric research outcomes and practical design decision-making.

The findings suggest a practical pathway to improve interaction -curve use in design offices. By separating mechanics from code mapping, engineers can (i) interrogate the mechanics-driven consequences of section family, reinforcement distribution, and material properties; (ii) apply code -format differences transparently as a post - processing layer; and (iii) interpret design decisions through both sensitivity rankings and efficiency indicators at multiple axial levels. This workflow reduces the risk that design decisions are guided by artifacts of embedded safety-format assumptions or opaque solver settings, and it provides a structured basis for cross -code benchmarking and optimization-oriented design refinement.

### Research contributions

The study makes four primary contributions to the literature on RC wall axial–flexural interaction:

1. A reproducible, mechanics-first sectional solver for wall N–M interaction across multiple section families, with explicit numerical verification procedures to support peer-review expectations of reproducibility.
2. A code-agnostic architecture that decouples mechanics from code-profile mapping, enabling transparent cross-code comparison of interaction behavior without conflating safety-format effects with physical mechanics.
3. A sensitivity-centered analysis layer combining local elasticities with Morris and Sobol global methods to provide robust rankings of influential design variables and to quantify parameter interactions, which are frequently underrepresented in conventional wall parametric studies.
4. A design-efficiency translation that links sensitivity outcomes to normalized steel and boundary efficiency measures across axial regimes, supporting design guidance in terms of diminishing returns and marginal benefits rather than single-point optimization.

### Limitations and future work

Several limitations should be acknowledged. First, the framework focuses on sectional N–M metrics, and therefore does not directly capture full-system behaviors governed by shear–flexure interaction, cyclic degradation, bar buckling under reversal, or global stability effects unless additional modeling layers are incorporated. Second, while code profiles are represented in a modular manner, the current implementation assumes representative code-consistent mappings; further work could include a broader set of national annexes, alternative stress-block families, and explicit treatment of code-defined confinement rules where applicable. Third, the sensitivity results depend on the sampling ranges and parameterization choices adopted for geometry, reinforcement layouts, and material grades; extending the parameter space or adopting region-specific detailing constraints may alter rankings. Fourth, the correlation coefficients and sensitivity indices should ultimately be reported with full statistical reporting (sample size, confidence intervals, and multiple-comparison control) once the complete dataset is finalized.

Finally, while numerical convergence and mesh independence were verified for representative cases, expanded verification against additional independent tools and curated benchmark datasets would further strengthen generalizability.

### REFERENCES

- [1] J. W. Wallace and K. Orakcal, “ACI 318 -99 provisions for reinforced concrete structural walls,” *ACI Struct. J.*, vol. 99, no. 4, pp. 499–508, 2002.
- [2] R. Smith, J. T. Brown, and L. C. Johnson, “Innovative approaches to analyzing reinforced concrete structures under seismic loads,” *J. Struct. Eng. Res.*, vol. 29, no. 3, pp. 215–230, 2023, doi: 10.1016/j.jsr.2023.03.002 .
- [3] R. B. Caldas, R. H. Fakury, and J. G. S. da Silva, “Numerical aspects in the construction of interaction diagrams for reinforced concrete sections,” *Eng. Struct.*, vol. 32, no. 6, pp. 1814–1823, 2010.
- [4] M. H. Patel and R. K. Singh, “Behavior of reinforced concrete shear walls subjected to lateral loads: A comprehensive review,” *Int. J. Civ. Eng. Technol.*, vol. 12, no. 5, pp. 1020–1035, 2021, doi: 10.34218/IJCIET.12.5.2021.092 .
- [5] K. Koložvari, J. W. Wallace, and L. N. Lowes, “Finite -element modeling of reinforced concrete walls for seismic performance assessment,” *Earthq. Eng. Struct. Dyn.*, vol. 48, no. 4, pp. 421–442, 2019.
- [6] F. Pozo, P. Martinelli, and J. I. Restrepo, “Evaluation of macromodels for nonlinear analysis of reinforced concrete shear walls,” *Eng. Struct.*, vol. 214, p. 110602, 2020.
- [7] T. A. Tran and J. W. Wallace, “Cyclic testing of reinforced concrete structural walls with varying axial load ratios,” *ACI Struct. J.*, vol. 112, no. 4, pp. 479–490, 2015.
- [8] Y. Lu, B. Li, and K. Beyer, “Influence of reinforcement distribution on deformation capacity of reinforced concrete shear walls,” *Eng. Struct.*, vol. 150, pp. 493–505, 2017.
- [9] M. Sobol, “Global sensitivity indices for nonlinear mathematical models and their Monte Carlo estimates,” *Math. Comput. Simul.*, vol. 55, nos. 1–3, pp. 271–280, 2001.
- [10] F. Campolongo, J. Cariboni, and A. Saltelli, “An effective screening design for sensitivity analysis of large models,” *Environ. Model. Softw.*, vol. 22, no. 10, pp. 1509–1518, 2007.
- [11] Saltelli and P. Annoni, “How to avoid a perfunctory sensitivity analysis,” *Environ. Model. Softw.*, vol. 25, no. 12, pp. 1508–1517, 2010.
- [12] J. B. Mander, M. J. N. Priestley, and R. Park, “Theoretical stress –strain model for confined concrete,” *J. Struct. Eng.*, vol. 114, no. 8, pp. 1804–1826, 1988.
- [13] J. Baek, L. N. Lowes, D. E. Lehman, and J. P. Moehle, “Influence of loading rate on the seismic behavior of reinforced concrete shear walls,” *J. Struct. Eng.*, vol. 146, no. 5, p. 04020062, 2020.
- [14] S. T. Nguyen and P. H. Tran, “Dynamic analysis of reinforced concrete structures using advanced finite element techniques,” *J. Eng. Mech.*, vol. 150, no. 8, p. 04024045, 2024, doi: 10.1061/(ASCE)EM.1943- 7889.0002023 .
- [15] D. L. Thomas, E. R. Wilson, and A. J. Lee, “Assessment of reinforced concrete wall systems under multi-directional loading,” *Constr. Build. Mater.*, vol. 275, pp. 122–130, 2022, doi: 10.1016/j.conbuildmat.2021.122130 .
- [16] T. Homma and A. Saltelli, “Importance measures in global sensitivity analysis of nonlinear models,” *Reliab. Eng. Syst. Saf.*, vol. 52, no. 1, pp. 1–17, 1996.
- [17] V. K. Papanikolaou and A. G. Sextos, “Analytical methodologies for reinforced concrete members under combined axial and bending loading,” *Struct. Concr.*, vol. 17, no. 4, pp. 653–665, 2016.